JOURNAL OF GEOPHYSICAL RESEARCH, VOL. 114, E04009, doi:10.1029/2008JE003287, 2009

Giant impacts on early Mars and the cessation of the Martian dynamo

J. H. Roberts,[1,2] R. J. Lillis,[3] and M. Manga[4]

Received 24 October 2008; revised 29 January 2009; accepted 11 February 2009; published 23 April 2009.

[1] Although Mars currently has no global dynamo-driven magnetic field, widespread crustal magnetization provides strong evidence that such a field existed in the past. The absence of magnetization in the younger large Noachian basins suggests that a dynamo operated early in Martian history but stopped in the mid-Noachian. Within a 100 Ma period, 15 giant impacts occurred coincident with the disappearance of the global magnetic field. Here we investigate a possible causal link between the giant impacts during the early and mid-Noachian and the cessation of the Martian dynamo at about the same time. Using three-dimensional spherical mantle convection models, we find that impact heating associated with the largest basins (diameters >2500 km) can cause the global heat flow at the core-mantle boundary to decrease significantly (10–40%). We suggest that such a reduction in core heat flow may have led to the cessation of the Martian dynamo.

Citation: Roberts, J. H., R. J. Lillis, and M. Manga (2009), Giant impacts on early Mars and the cessation of the Martian dynamo, *J. Geophys. Res.*, *114*, E04009, doi:10.1029/2008JE003287.

1. Introduction

[2] Mars currently has no global dynamo-driven magnetic field, but the existence of strong crustal fields due to remanent magnetization [*Acuña et al.*, 2001] indicates that a global field existed in the past. The absence of magnetization in the large basins Hellas and Argyre suggests that a dynamo operated during the early to mid-Noachian epoch, but stopped soon thereafter [*Acuña et al.*, 1999; *Arkani-Hamed and Boutin*, 2004].

[3] Recent simulations of the Martian dynamo indicate that it may have been in a subcritical regime early in Martian history [*Kuang et al.*, 2008]. A subcritical dynamo occurs in a fluid iron core that has insufficient thermal forcing to initiate convection and generate a magnetic field on its own, but can sustain convection in the presence of a preexisting magnetic field. In this situation, a decrease in CMB heat flow of as little as 1% can be sufficient to shut down the global magnetic field [*Kuang et al.*, 2008]. In order to restart the dynamo, the core dynamo must become supercritical, requiring an increase in heat flow of ~25% above the minimum needed to sustain the subcritical dynamo. Thus, if the dynamo fails once, it may not return even if the original core cooling rate is restored. Other studies suggest that the early Martian dynamo may have operated only in a single hemisphere as an effect of the formation of the hemispheric dichotomy [*Stanley et al.*, 2008]. A single-hemisphere dynamo may explain the concentration of magnetization in the southern highlands, but does not address the presence of local regions of moderate magnetization in the north [*Johnson and Phillips*, 2005], or the timing of the dynamo's cessation.

[4] Observations of gravity and topography [*Frey*, 2008] indicate that 15 of the 20 giant (i.e., basins >1000 km in diameter) ancient Martian impacts occurred within a 100 Ma period, toward the end of which the global magnetic field disappeared [*Lillis et al.*, 2008a]. Further, the five unambiguously demagnetized basins are also the youngest of the 20. Utopia, perhaps the oldest of these demagnetized basins (see Figure 1), is also the largest and therefore has the greatest potential to affect the interior.

[5] These impacts have the potential to deliver significant amounts of heat to the mantle [*Reese et al.*, 2002; *Monteux et al.*, 2007; *Watters et al.*, 2009]. The cessation of the dynamo is usually attributed to a heat flow at the core-mantle boundary (CMB) that is too low to permit core convection [*Nimmo and Stevenson*, 2000]. Here we investigate a possible link between the giant impacts during the early and mid-Noachian and the cessation of the Martian dynamo at or about the same time. We determine the heating of the Martian mantle due to impactors [*Watters et al.*, 2009] that formed the twenty largest extant and buried impact basins with diameters greater than 1000 km [*Frey*, 2008]. At model times corresponding to the Hartmann-Neukum ages of the impact basins [*Hartmann and Neukum*, 2001; *Frey*, 2008] we introduce this impact heating into 3D spherical convection models [*Zhong et al.*, 2000; *Tan et al.*, 2006] of the Martian mantle. We then examine the effect of this heating on the CMB heat flow.

[6] First, we give a short background of the observations of the giant impact basins on Mars, their ages and magnetization states, and the early dynamo. Next, we describe our

[1]Department of Earth and Planetary Sciences, University of California, Santa Cruz, California, USA.
[2]Now at Johns Hopkins University Applied Physics Laboratory, Laurel, Maryland, USA.
[3]Space Sciences Laboratory, University of California, Berkeley, California, USA.
[4]Department of Earth and Planetary Science, University of California, Berkeley, California, USA.

0148-0227/09/2008JE003287$09.00

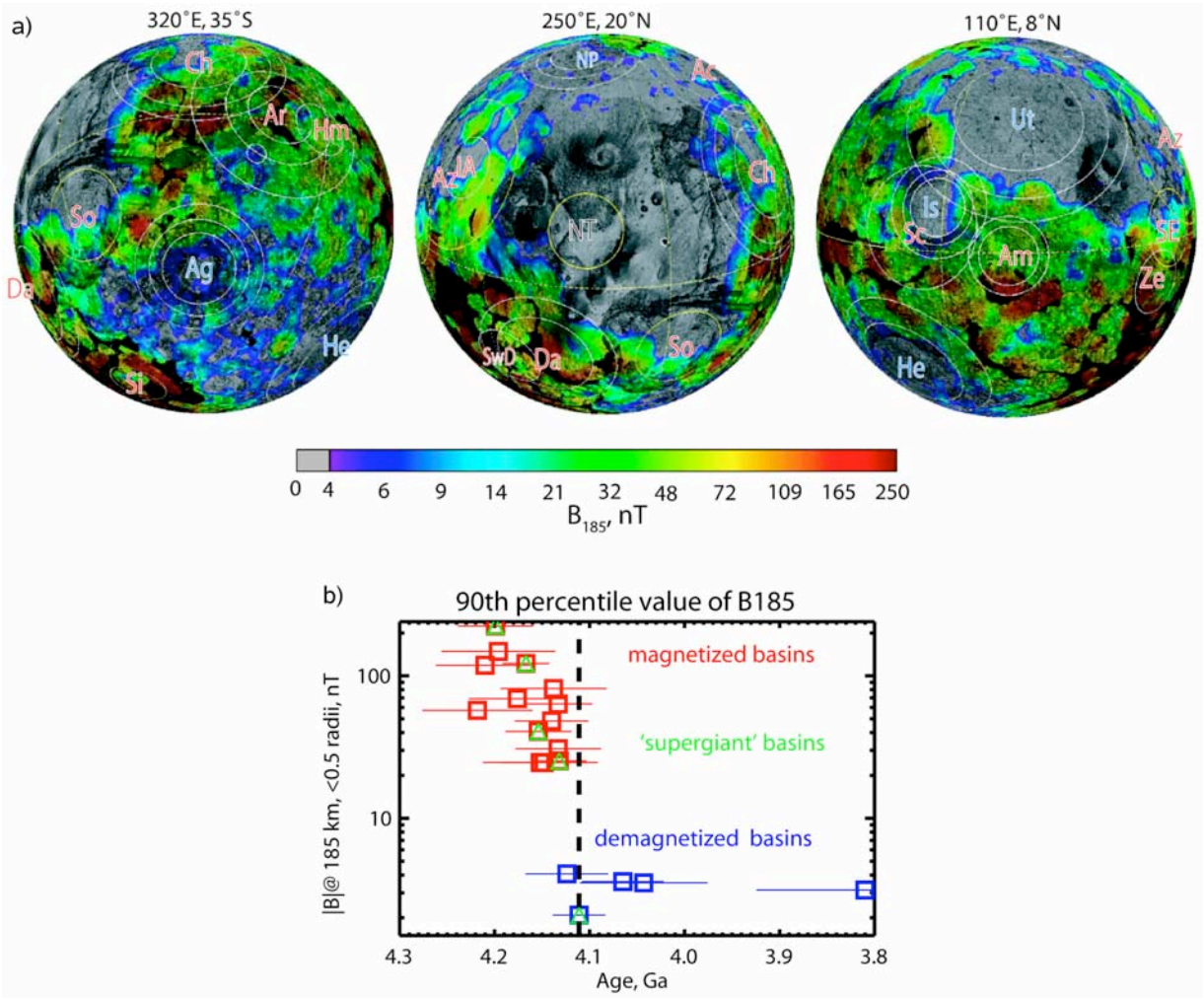

Figure 1. (a) Orthographic maps of crustal magnetic field magnitude at 185 km altitude (denoted B185; note logarithmic scale) overlaid on shaded MOLA topography, adapted from *Lillis et al.* [2008a]. The 20 largest basins identified in topographic and crustal thickness data are shown as white and yellow circles, respectively. Each ring in multiringed basins is shown. Demagnetized and magnetized basins are identified with blue and red lettering, respectively. (b) The 90th percentile of the distribution of 0.5° × 0.5° pixels of B185 inside 0.5 basin radii is plotted against absolute model ages [*Hartmann and Neukum*, 2001; *Frey*, 2008] for all identified basins except North Tharsis (thermally demagnetized). The five largest basins are also marked with green triangles. Note that the youngest basins (i.e., North Polar, Utopia, Hellas, Argyre, and Isidis) are the least magnetized.

methods for computing the mantle heating due to the impacts and our models of mantle convection incorporating this heating. In section 5, we present the results of our models for a range of mantle viscosities and radioactive heating rates, with particular attention to the spatial and temporal variation of the CMB heat flow. Finally, we discuss the implications of our results for the cessation of the Martian dynamo and the loss of the global magnetic field.

2. Giant Impacts

[7] Quasi-circular depressions (QCDs) identified in MOLA topography [*Frey et al.*, 2002] and circular thin-crust areas (CTAs) identified in crustal thickness maps [*Neumann et al.*, 2004] have been associated with both exposed and buried impact structures [*Frey et al.*, 2007; *Frey*, 2008]. The combined population of QCDs and CTAs provides the best estimate available of the N(300) crater retention ages (CRAs) for large Martian basins [*Frey*, 2008]. N(x) is the cumulative number of superimposed craters of diameter > x km per 10^6 km^2. CRAs of the large basins show a strong clustering between N(300) = 2.5 and 4.0 (or 4.1 and 4.2 Gyr in model age [*Hartmann and Neukum*, 2001]), implying a "peak" in crater production that may correspond to the Late Heavy Bombardment [*Gomes et al.*, 2005]. However, a recent study [*Arkani-Hamed*, 2009] notes that many of the giant impacts trace great circles that may correspond to paleoequators [*Arkani-Hamed*, 2001], and suggests that the impactors were initially retrograde satellites whose orbits decayed.

[8] We take from *Frey* [2008] the times, locations and sizes of the 20 largest impacts. These are summarized in Table 1 and in Figure 1. We have chosen the "primary" diameter D_{basin} for all multiring basins, defined by *Frey*

Table 1. Noachian Giant Impact Basins on Mars

Name	Abbreviation	Long. (°E)	Lat. (°N)	D (km)	N(300)	Model Age (Ga)
Amenthes	Am	110.6	−0.9	1070	6.68	4.218
Zephyria	Ze	164.3	−12.4	1193	6.27	4.210
Daedalia	Da	228.3	−26.5	2639	5.70	4.199
Sirenum	Si	205.3	−67.4	1069	5.57	4.196
SW Daedalia	SW	213.9	−29.4	1278	4.68	4.176
Ares	Ar	343.9	4.0	3300	4.33	4.167
Amazonis	Az	187.9	27.1	2873	3.86	4.154
In Amazonis	IA	192.5	29.3	1156	3.81	4.152
Solis	So	275.3	−23.8	1663	3.68	4.148
N Tharsis	NT	243.6	17.6	1347	3.51	4.143
Chryse	Cr	318.0	25.0	1725	3.42	4.140
Hematite	Hm	357.8	3.2	1065	3.37	4.138
Scopolus	Sc	81.8	6.9	2250	3.24	4.133
SE Elysium	SE	170.3	3.7	1403	3.24	4.133
Acidalia	Ac	342.7	59.8	3087	3.21	4.132
North Polar	NP	195.2	80.0	1600	2.99	4.124
Utopia	Ut	115.5	45.0	3380	2.68	4.111
Hellas	He	66.4	−42.3	2070	1.78	4.065
Argyre	Ag	317.5	−49.0	1315	1.47	4.043
Isidis	Is	87.8	13.4	1352	0.17	3.810

[2008] as the clearest circular topographic feature, and therefore the most likely to reflect the transient cavity diameter D_{tr} immediately after impact before gravity-driven relaxation. We note that there remains some uncertainty in the D_{basin}/D_{tr} scaling [*McKinnon et al.*, 2003], particularly for large basins. This leads to uncertainty about the impactor size and the amount of heating deposited in the mantle. *Melosh* [2008] points out that the energy required to open a very large crater against gravity consumes a large fraction of the total available energy, and therefore scaling relations predict the ratio between D_{basin} and projectile size (and therefore D_{tr}) decreases with increasing crater size. Additionally, recent hydrocode simulations indicate that large basins collapse less than most predictions (L. E. Senft and S. Stewart, Transiently weak faults drive impact crater collapse, submitted to Nature, 2008). For these reasons, we use the scaling of *Holsapple* [1993] with a relatively weak exponential dependence (S. Stewart, personal communication, 2008) in our models. The final and transient cavity diameters are related by

$$D_{basin} = 1.02 D_c^{-0.086} D_{tr}^{1.086}, \quad (1)$$

where D_c is the simple-to-complex transition diameter [*Holsapple*, 1993], and is ∼7 km for Mars [*Melosh*, 1989]. Because of the aforementioned scaling uncertainty, we have also run a case using the relation of *McKinnon and Schenk* [1985], with a stronger exponential dependence of 1.13. We have also explored the extreme situation where $D_{basin} = D_{tr}$.

[9] We do not consider the effects of the putative Borealis basin-forming impact that may have been responsible for the hemispheric dichotomy [*Andrews-Hanna et al.*, 2008; *Marinova et al.*, 2008; *Nimmo et al.*, 2008]. The dichotomy is far older [*Nimmo and Tanaka*, 2005] than the basins in Table 1. The time between the dichotomy formation and the first impact that we study (Amenthes) is several mantle-crossing times, and we expect any lateral thermal anomalies due to such an event to have been erased. The Borealis impact, if it occurred, is therefore equivalent to a slightly warmer initial condition in our models.

[10] Immediately after a large impact, magnetized crust is excavated and the underlying material is shocked and heated, removing magnetization over an area approximately the size of the final basin diameter [*Hood et al.*, 2003] and throughout the entire depth of crust [*Shahnas and Arkani-Hamed*, 2007]. When the crust within the basin cools below the Curie temperature(s) of its magnetic mineral(s), it acquires a thermoremanent magnetization proportional to the strength of the ambient magnetic field [*O'Reilly*, 1984]. For the basins 1000 km in diameter and greater which we examine, the crustal magnetic field at 185 km (B_{185}) [*Lillis et al.*, 2008b] serves as an reliable proxy for magnetization within the basin [*Lillis et al.*, 2008a], as shown in Figure 1. Note that B_{185} over the five youngest basins is at least an order of magnitude weaker than that over the older basins. Accounting for basin age uncertainty, this suggests that the dynamo-driven global magnetic field most likely ceased sometime between the Acidalia and Utopia impacts.

3. Impact Heating

[11] An impact sufficiently large to create and demagnetize the observed impact basins (see Figure 1) will introduce a substantial amount of heat into the interior of the planet. Neglecting the effects of planetary curvature, the basin and impactor diameters are related by

$$D_{imp} = 0.69 D_{tr}^{1.27} g^{0.28} v_i^{-0.56}, \quad (2)$$

where g is the gravity and v_i is the impact velocity [*Melosh*, 1989], assuming the same density for both bodies. A significant fraction of the impactor's kinetic energy will be converted to thermal energy, raising the temperature of the surrounding mantle and melting a sizable region.

[12] We follow the method of *Watters et al.* [2009], in which the mantle is heated by a shock wave emanating from the impact location at a depth $d_c = 0.305 R v_i^{0.361}$, where R is the impactor radius and v_i is in km/s. Heating is uniform within an isobaric core with radius $r_c = 0.451 R v_i^{0.211}$ and

Table 2. Global Parameters

Parameter	Symbol	Value
Reference density	ρ_0	3500 kg m^{-3}
Gravitational acceleration	g	3.7 m s^{-2}
Coefficient of thermal expansion	α	3×10^{-5} K^{-1}
Surface temperature	$T_{surface}$	220 K
CMB temperature	T_{CMB}	2220 K
Planetary radius	R_0	3400 km
Coefficient of thermal diffusion	κ	10^{-6} m^2 s^{-1}
Impact velocity	v_i	15 km s^{-1}
	C	7.24 km s^{-1}[a]
	S	1.25[a]
Thermal conductivity	k	4.2 W m^{-1}K^{-1}

[a] *Watters et al.* [2009].

decays rapidly outside this region. For v_i = 15 km/s as used in this study, $d_c \approx r_c$. We parameterize the impact heating as a temperature perturbation ΔT in the mantle [*Reese et al.*, 2002; *Monteux et al.*, 2007; *Watters et al.*, 2009], as a function of the shock pressure P_s:

$$\Delta T(P_s) = \frac{P_s}{2\rho_0 S}\left(1 - f^{-1}\right) - (C/S)^2(f - \ln f - 1) \quad (3)$$

$$f = -\frac{2SP_s}{C^2\rho_0}\left(1 - \sqrt{\frac{4SP_s}{C^2\rho_0} + 1}\right)^{-1} \quad (4)$$

where ρ_0 is the background mantle density, and C and S are constants based on the mantle material properties, assuming a Tillotson equation of state [*Melosh*, 1989; *Watters et al.*, 2009]. See Table 2 for parameter values. The shock pressure is defined [*Watters et al.*, 2009] as

$$P_s(r) = \begin{cases} \rho_0(C + Su_c)u_c & r \le r_c, \\ P_s(r_c)(r_c/r)^{-1.84+2.61\log v_i} & r > r_c. \end{cases} \quad (5)$$

where the particle velocity $u_c = v_i/2$, when the target and impactor have the same density as assumed here. This temperature increase may result in a melt region several times the size of the isobaric core. However, convection is very efficient in a liquid, and the magma pond will solidify quickly compared to the dynamical time scale of the solid mantle. Therefore, again following *Watters et al.* [2009], we set the temperature in the mantle to the solidus temperature T_{sol} at all points where $T + \Delta T$ exceeds this value. We parameterize the solidus as

$$T_{sol} = 1374\text{K} + 130\text{K GPa}^{-1}P - 5.6\text{K GPa}^{-2}P^2, \quad (6)$$

where P is the lithostatic pressure [*Reese et al.*, 2002].

[13] Because we assume the magma pond solidifies quickly, we do not include the latent heat of fusion in our heating model, and assume that it escapes to space. In reality, partial melt may persist for longer times [*Watters et al.*, 2009], resulting in a slow release of latent heat into the mantle. Therefore our results are a lower bound on the magnitude of the thermal perturbation resulting from impacts. We also assume the magma pond does not deform substantially. On sufficiently long time scales, the topography at the base of the melt region may relax, allowing the buoyant magma to spread out into a global ocean [*Tonks and Melosh*, 1992; *Reese and Solomatov*, 2006]. However, this time scale is controlled by the viscosity of the surrounding mantle and is long compared to the circulation time of the magma. Furthermore, deformation of the melt zone could not have happened to a very large extent or the impact basin would have been erased.

4. Convection Modeling

[14] We model thermal convection in the Martian mantle using the three-dimensional spherical finite element convection code CitcomS [*Zhong et al.*, 2000; *Tan et al.*, 2006]. Our model domain contains 1.8 million elements. We use a temperature- and pressure-dependent viscosity, and apply isothermal and free-slip boundary conditions at the surface and core-mantle boundary (CMB). Secular cooling of the core is included on the basis of the CMB heat flow; thus the CMB temperature drops over time. We assume an initially convecting mantle with an adiabatic interior and apply a small spherical harmonic degree 20 perturbation to the temperature field. We use the extended Boussinesq approximation [*Christensen and Yuen*, 1985] and included internal heating from radioactive decay [*Wanke and Dreibus*, 1994]. At the times indicated by the impact age model described above (and Table 1 of *Frey* [2008]), we apply an instantaneous temperature increase ΔT, whose spatial distribution is defined by equation (3), centered on the location of the corresponding impact at depth d_c. Values for model parameters are given in Table 2.

[15] We have run a series of models in which we vary the convective vigor (parameterized by the Rayleigh number *Ra*) and radioactive heating rate Q_0. Each model was run for ~3 Ga, until well after the last large impact (Isidis) had occurred. In order to examine the effect the impacts have on the thermal evolution, we also ran a control case for each set of parameters in which the impact heating was not included. Model parameters specific to each case are given in Table 3.

5. Results

[16] The global surface and core-mantle boundary (CMB) heat flow for four pairs of models are plotted in Figures 2a–2d. While every impact causes a spike in surface heat flow, only the very largest impactors (D > 2500 km) create a noticeable perturbation at the CMB. Only this group of "supergiant" impactors generate heated regions that are large enough to intersect or approach the CMB (see, e.g., Figures 6b and 7). The thermal perturbation dies off very quickly with distance from the isobaric core. Heating of the shallower mantle by the smaller impacts is not sufficient to dampen the global CMB heat flow significantly. The excess heat is advected to the surface and lost to space faster than the thermal perturbation can extend its influence downward. Supergiant impacts, however, can have a very strong impact on the CMB heat flow, reducing it by up to 10% for case 2 (Figure 2c) and by 40% for case 6 (Figure 2d) because of the lower background heat flux. These impacts have such a large effect because they can impart very large temperature changes at the bottom of the mantle, up to ~200 K limited only by the mantle solidus. Because the mantle is in the stagnant lid regime, this is comparable to the temperature

Table 3. Model-Specific Parameters

Case	*Ra*	Q_0 (W m^{-3})	Impacts?	Scaling	$\delta F_{CMB,Ut}$ (%)
1	3.05×10^7	6.2×10^{-8}	no	-	—
2	3.05×10^7	6.2×10^{-8}	yes	*Holsapple* [1993]	9.2
2a	3.05×10^7	6.2×10^{-8}	yes	*McKinnon and Schenk* [1985]	2.0
2b	3.05×10^7	6.2×10^{-8}	yes	none	248
3	3.05×10^7	3.1×10^{-8}	no	-	—
4	3.05×10^7	3.1×10^{-8}	yes	*Holsapple* [1993]	10.6
5	6.1×10^6	6.2×10^{-8}	no	-	—
6	6.1×10^6	6.2×10^{-8}	yes	*Holsapple* [1993]	43.0
7	6.1×10^6	3.1×10^{-8}	no	-	—
8	6.1×10^6	3.1×10^{-8}	yes	*Holsapple* [1993]	27.8

difference across the lower thermal boundary layer [*Jellinek et al.*, 2002], and thus has a large effect on the global CMB heat flow, even when only a portion of the deep mantle is substantially heated. Spatial variations in the heat flow due to an impact are also quite large. In Figure 3, we plot the standard deviation of the heat flow for case 2. This is low during quiescent periods, but spikes whenever an impact occurs. Buoyancy resulting from the impact heating also drives very strong increases in velocity (Figure 4), as the warm material rises through the mantle.

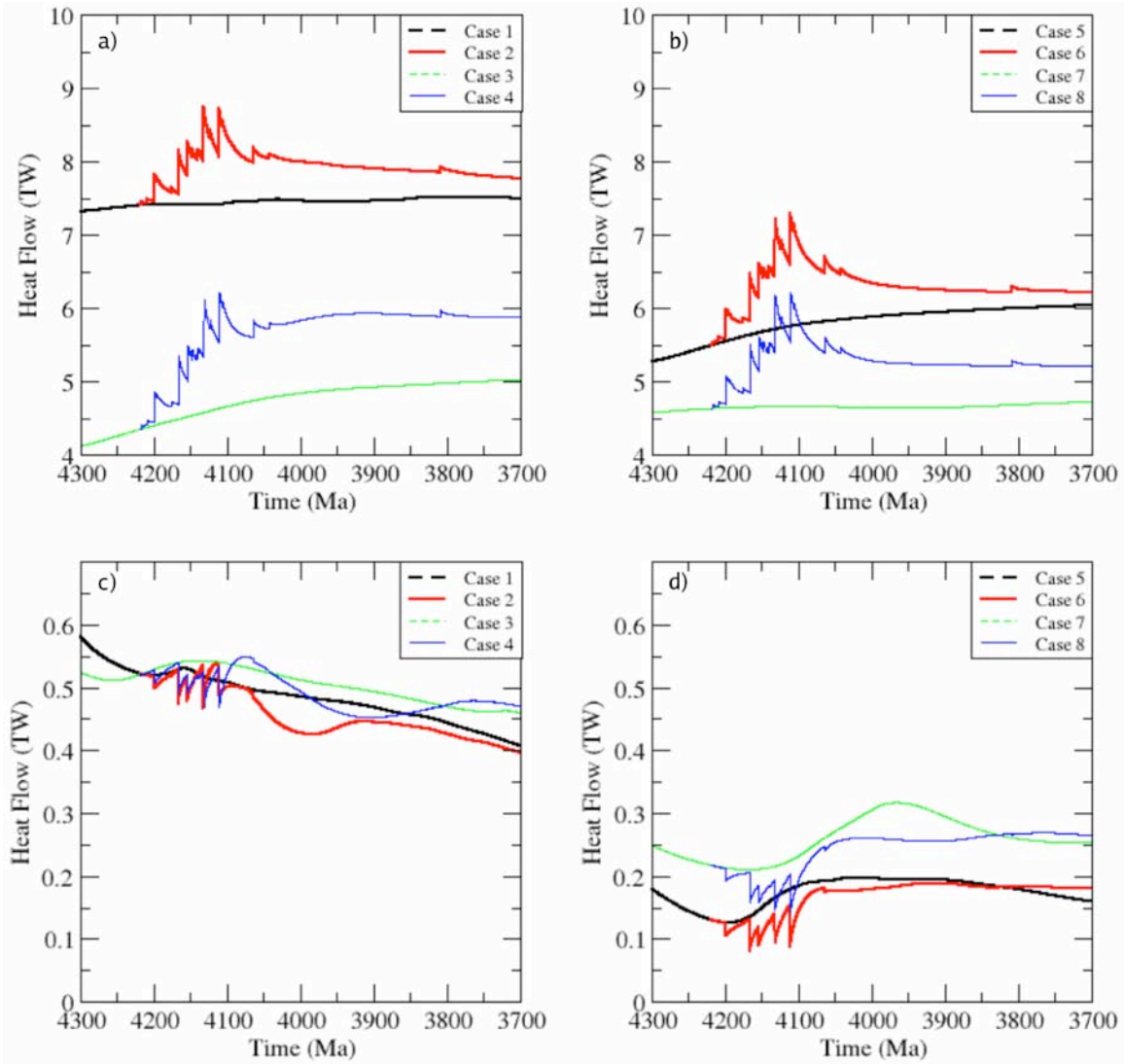

Figure 2. (a and b) Total global heat flow at the surface and (c and d) CMB versus time for cases 1–4 with $Ra = 3.05*10^7$ (Figures 2a and 2c) and cases 5–8 with $Ra = 6.1*10^6$ (Figures 2b and 2d). Each impact causes a strong perturbation to the surface heat flow. Relatively little heat is deposited at large depths. Only impactors forming basins >2500 km in diameter cause a significant drop in the CMB heat flux, but these drops can be large (>10–40%).

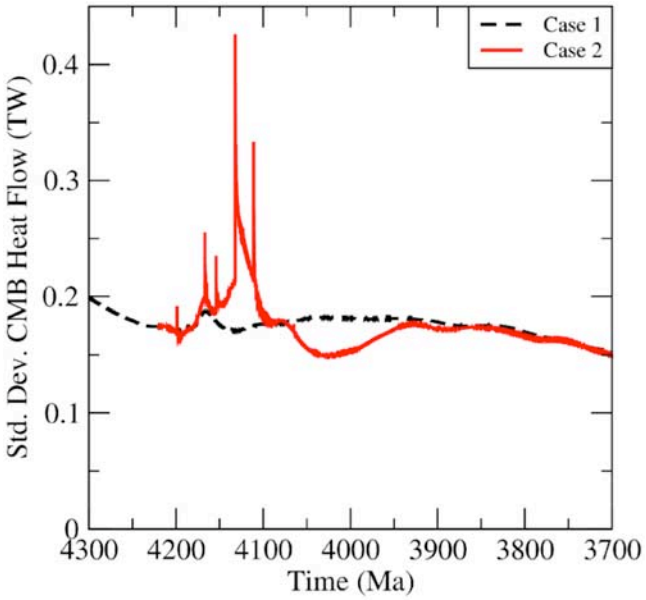

Figure 3. Standard deviation of spatial variation of CMB heat flow versus time for cases 1 and 2.

[17] The results for all cases with impacts (Table 3), are qualitatively similar to case 2. The heat flow is sharply reduced at the CMB, provided the impact is large enough to generate a significant temperature increase at that depth. The decrease in CMB heat flow due to the mantle heating outweighs any increase that may develop because of enhanced buoyancy caused by lateral temperature variations. The buoyancy may become important during the recovery period, when the CMB heat flow may temporarily attain a slightly higher value than the corresponding control case. *Ra* is an important control on the ability of the mantle to recover the preimpact cooling rate. Case 6 is identical to case 2 except for a factor of 5 reduction in *Ra*. Because convection is more sluggish, it takes longer to remove the impact heat and return the CMB heat flow to the preimpact value. In Figure 5, we plot the difference in CMB heat flow between cases 1 and 2 and between cases 5 and 6 for the period of most intense bombardment, 4.2–4.1 Ga. In case 2 (thick line), the heat flow anomaly returns to 0 on a time scale of ~30 Ma, and may temporarily change sign because of the buoyancy of the deep heated material. In case 6 (thin line), the heat flow anomaly does not return to 0 before the next giant impact, and the anomalies from successive impacts accumulate. The fractional change in CMB heat flow due to the Utopia impact, $\delta F_{C,Ut}$ for each case is given in the last column of Table 3.

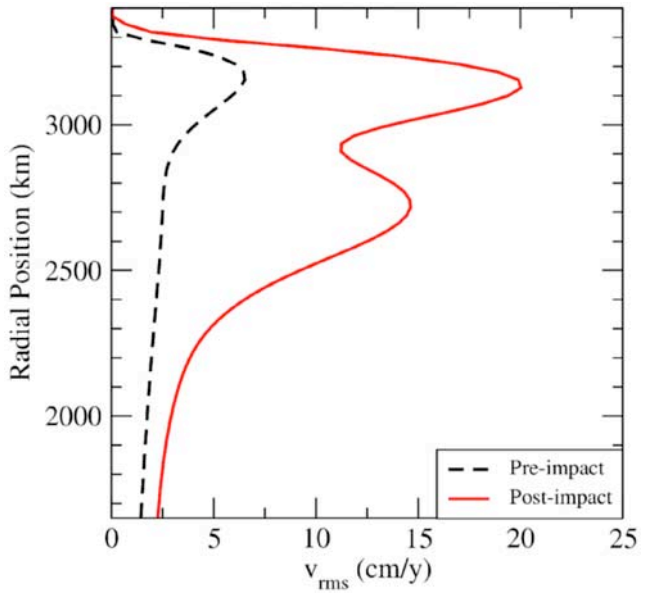

Figure 4. Horizontally averaged RMS velocity versus depth before and after the Utopia impact for case 2.

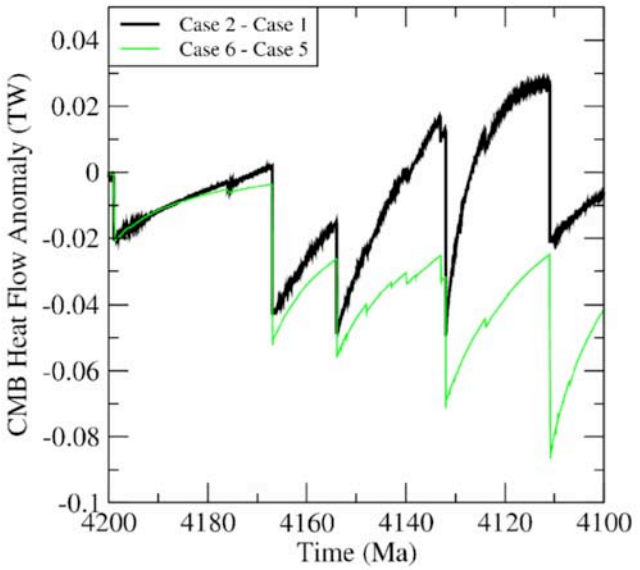

Figure 5. CMB heat flow anomalies for cases 2 and 6 relative to their respective reference cases 1 and 5 for the period of most intense bombardment. Impacts with $D >$ 2500 km are marked; see Table 1 for abbreviations. The more viscous mantle in case 6 cannot remove the impact heating as effectively as in case 2 and takes longer to restore the original heat flow.

[18] In addition to the substantial effect on the heat flow, impact heating can dominate the large-scale flow structure. Figure 6 shows 6 snapshots of the mantle temperature immediately before and up to 8 Ma after the Utopia impact (see auxiliary material Animation S1).[1] Figure 6a shows the preexisting pattern of thermal upwellings in a vertical slice through the center of Utopia. A temperature increase due to the impact is introduced (Figure 6b). The impact-heated region rises and spreads out beneath the lithosphere. The plume head spreads out beneath the stagnant lid, presenting a greater surface area to the cold lithosphere and begins to cool (Figures 6c–6e). The nearby preexisting upwelling is advected toward the deep warm impact-heated region, shifting the overall convective pattern (Figure 6f). Instabilities in the cold lid penetrate the cooling plume cap, reducing the surface heat flow, but the anomaly takes ~30 Ma to fully dissipate.

[1] Auxiliary materials are available in the HTML. doi:10.1029/2008JE003287.

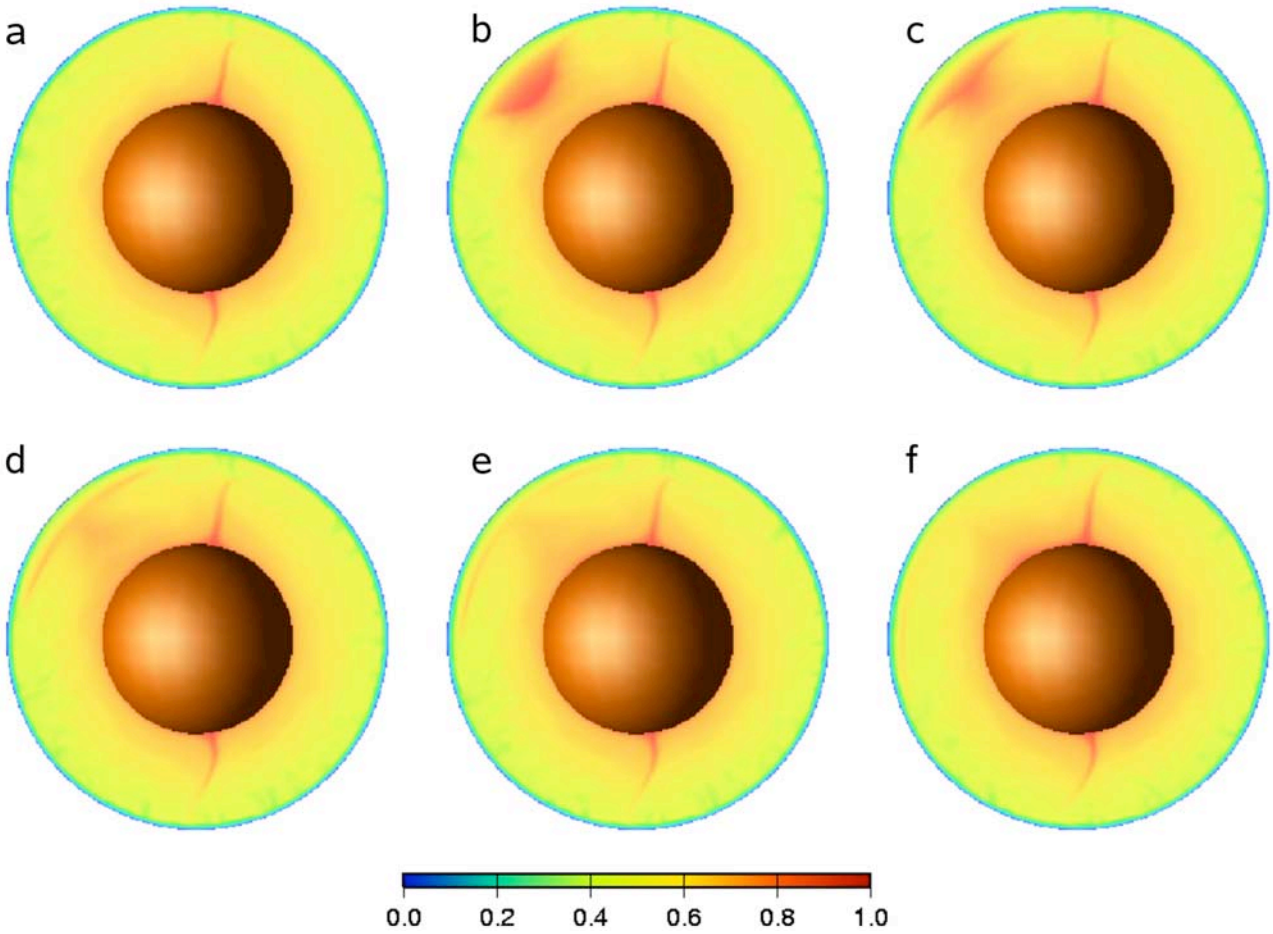

Figure 6. Evolution of nondimensional temperature field due to Utopia impact in case 2. Shown are cross sections through the impact site. (a) Preexisting upwellings. Ut − 1.9 Ma. (b) Addition of thermal perturbation due to impact heating. Ut − 0. Impact heated material rises and spreads out beneath lithosphere. As plume cap cools, instabilities form in cold lid. Downwellings form. (c) Ut + 0.3 Ma. (d) Ut + 1.7 Ma. (e) Ut + 4.2 Ma. (f) Plume head fades; surface heat flow drops. Ut + 7.8 Ma.

[19] We have also explored the effect of the $D_{basin} - D_{tr}$ scaling law on the impact heating. We repeated case 2 using the *McKinnon and Schenk* [1985] scaling and find that owing to the smaller transient cavity, the effect on the heat flow is reduced. This results in a Utopia anomaly of about 2%. This is still technically sufficient to shut off a subcritical dynamo, but requires a narrow range for the preimpact heat flow. In the case where the transient and final basin diameters are equal, we find much stronger impact heating. In this situation, the largest (D > 3000 km) impacts may cause the global heat flow to change sign, heating the core from above, which should be sufficient to at least temporarily shut off even a supercritical dynamo. This difference in heating is illustrated in Figure 7, in which the temperature profiles due to the Utopia impacts is shown for the different scaling laws for case 2, as well as the global CMB heat flow for all scaling relations for the period of most intense bombardment (4.2–4.1 Ga).

6. Discussion and Conclusions

[20] We find that mantle heating due to largest impacts that form basins with diameters greater than 2500 km on early Mars can substantially reduce the CMB heat flow. This reduction in the efficiency of core cooling may have profound effects on the dynamo-driven magnetic field. The ancient global magnetic field on Mars (as on Earth) was likely generated by convection in the fluid core, although a recent study [*Arkani-Hamed*, 2009] suggests it may have been powered by tidal excitation of retrograde satellites. The vigor of core convection is largely controlled by the heat flow at the CMB. *Nimmo and Stevenson* [2000] estimate that ~0.5 TW is required in order to sustain core convection. Once the heat flow becomes unfavorable, the magnetic field can dissipate effusively in a geologically rapid time of ~5–20 ka (calculated using arguments from *Stevenson* [2003]), which is short compared to the duration of the spikes in heat flow (Figure 2). Although the CMB heat flow tends to return to its background value postimpact within ~30 Ma (Figure 2), the magnetic field will not necessarily recover to the original strength. Below, we present two scenarios in which giant impacts lead to the cessation of the Martian dynamo.

6.1. Subcritical Dynamo

[21] Recent simulations of the Martian dynamo indicate that it may have been in a subcritical regime early in

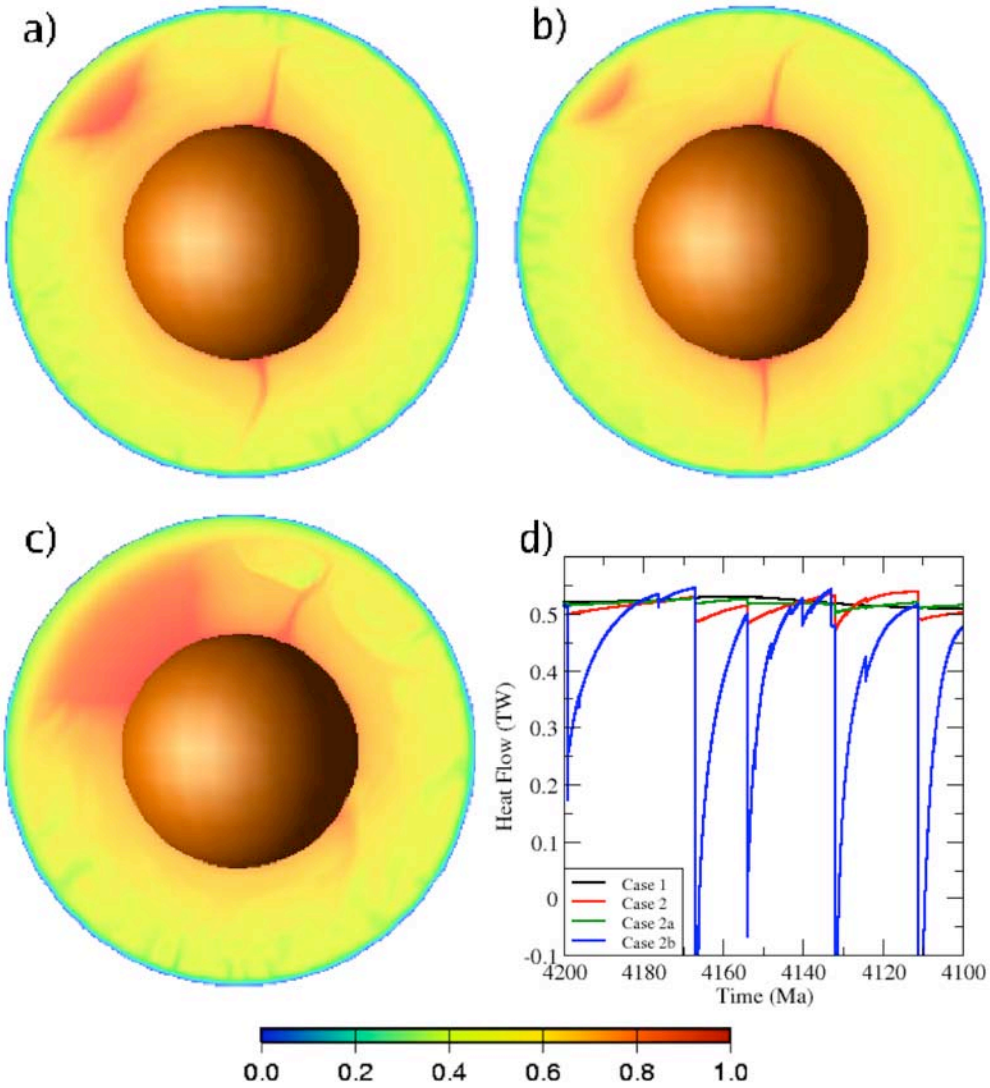

Figure 7. Nondimensional temperature field immediately after Utopia impact in case 2 for three different scaling laws. (a) *Holsapple* [1993]. (b) *McKinnon and Schenk* [1985]. (c) No scaling, $D_{basin} = D_{tr}$. (d) CMB heat flow versus time for the period of most intense bombardment for case 1 and case 2 using three different scaling laws for D_{basin}/D_{tr}.

Martian history [*Kuang et al.*, 2008]. A subcritical dynamo occurs in a fluid iron core that has insufficient thermal forcing to initiate convecting and generate a magnetic field on its own, but can sustain convection in the presence of a preexisting magnetic field. When no magnetic field is present, the Coriolis force must be balanced by viscous shear, and convection is suppressed. When a magnetic field is present, the Lorentz forces counter the Coriolis deflections, reducing the critical Rayleigh number Ra_c for convection. Thus an existing magnetic field allows convection and the field itself to be sustained with weaker thermal forcing than is required to initiate such convection in the absence of such a field [*Eltayeb and Roberts*, 1970]. *Kuang et al.* [2008] parameterize the vigor of core convection in terms of the *Ra* of the core, and find that this subcritical regime is quite narrow. The magnetic field strength is relatively insensitive to *Ra* above some subcritical value, but drops off sharply below this value. If the dynamo is in the subcritical regime, a decrease in CMB heat flow of as little as 1% can shut down the global magnetic field [*Kuang et al.*, 2008]. In order to restart the dynamo, the core dynamo must become supercritical, requiring an increase in heat flow of ~25% above the minimum needed to sustain the subcritical dynamo. Thus, if the dynamo fails once, it may not return even if the original core cooling rate is restored.

[22] Utopia is the largest and the oldest demagnetized basin, and thus may have been the impact to cause the critical decrease in CMB heat flow. Why the older, comparably sized Ares or Acidalia impacts did not cause the death of the dynamo is uncertain. The time needed to dissipate the heat from each impact is greater than the interval between impacts, particularly for cases with low *Ra*. Another control on the core cooling rate is the initial temperature. It is

possible that Ares and Acidalia did temporarily stop the dynamo, but that the dynamo was not subcritical at the time of these impacts and was able to restart once the background cooling was restored. If the core was initially very hot [*Williams and Nimmo*, 2004], the secular cooling may have carried the background heat flow below some critical value by the time of the Utopia impact, and the consequent subcritical dynamo was thus susceptible to being permanently shut down by the impact heating. This scenario relies on a rather specific set of initial conditions to make the dynamo subcritical at the time of Utopia. It is likely that the dynamo would have eventually shut down on its own (as in the work of *Nimmo and Stevenson* [2000]), and that the impact merely hastened it somewhat. However, such restrictions on the dynamo's criticality may not be necessary. Below, we present an alternative.

6.2. Supercritical Dynamo

[23] We note that the magnetization strength of the five supergiant impact basins ($D > 2500$ km) monotonically decreases with time (Figure 1b). For example, Daedalia has the strongest magnetization of the five, and Utopia has the weakest. This progression suggests an alternate scenario in which the dynamo need not be in the subcritical regime in order to be stopped by supergiant impacts.

[24] The heat flow drops seen in our models are quite significant (>40% in some models). This is in excess of the relatively narrow range that corresponds to a subcritical dynamo. Furthermore, the giant impacts generate strong lateral variations in CMB heat flow (see Figure 3) that may disrupt the preexisting core flow pattern and stop the dynamo, even if the global CMB heat flow is still favorable to convection [*Olson and Christensen*, 2002]. Thus, a single supergiant impact may be able to stop a relatively weak, but still supercritical dynamo. Although core convection will be able to restart once the thermal pulse from the impact dissipates, the magnetic field may not return to the original strength. In this scenario, four supergiant impacts cause the dynamo to fail and restart, ratcheting down the magnetic field strength. Finally, the Utopia impact shuts down the severely weakened dynamo and it is never able to recover.

6.3. Climate Change

[25] Mineralogy and stratigraphy observed with the OMEGA instrument is consistent with a climatic shift from wet to drier, more acidic conditions (the Phyllosian-Theiikian transition) during the Noachian era [*Bibring et al.*, 2006]. This shift happened prior to the Isidis impact [*Mustard et al.*, 2007] and may have occurred after the dynamo cessation [*Lillis et al.*, 2008b].

[26] **Acknowledgments.** This research was supported by NASA grants NNX07AL30G and NNX08AN13G, and by the Miller Institute. The authors would like to thank Herb Frey, Weijia Kuang, Francis Nimmo, and Erik Asphaug for discussions which improved this manuscript, the CIG for the Pyre-framework version of CitcomS, and two anonymous reviewers for their constructive comments.

References

Acuña, M. H., et al. (1999), Global distribution of crustal magnetization discovered by the Mars Global Surveyor MAG/ER Experiment, *Science*, *284*, 790–793.

Acuña, M. H., et al. (2001), Magnetic field of Mars: Summary of results from the aerobraking and mapping orbits, *J. Geophys. Res.*, *106*(E10), 23,403–23,417.

Andrews-Hanna, J. C., M. T. Zuber, and W. B. Banerdt (2008), The Borealis basin and the origin of the Martian crustal dichotomy, *Nature*, *453*, 1212–1215, doi:10.1038/nature07011.

Arkani-Hamed, J. (2001), Paleomagnetic pole positions and pole reversals of Mars, *Geophys. Res. Lett.*, *28*, 3409–3412.

Arkani-Hamed, J. (2009), Did tidal deformation power the core dynamo of Mars?, *Icarus*, in press.

Arkani-Hamed, J., and D. Boutin (2004), Paleomagnetic poles of Mars: Revisited, *J. Geophys. Res.*, *109*, E03011, doi:10.1029/2003JE002229.

Bibring, J. P., et al. (2006), Global mineralogical and aqueous Mars history derived from OMEGA/Mars Express data, *Science*, *312*, 400–404.

Christensen, U. R., and D. A. Yuen (1985), Layered convection induced by phase transitions, *J. Geophys. Res.*, *90*, 10,291–10,300.

Eltayeb, I. A., and P. H. Roberts (1970), On the hydromagnetics of rotating fluids, *Astrophys. J.*, *162*, 699–701.

Frey, H. (2008), Ages of very large impact basins on Mars: Implications for the Late Heavy Bombardment in the inner solar system, *Geophys. Res. Lett.*, *35*, L13203, doi:10.1029/2008GL033515.

Frey, H. V., J. H. Roark, K. M. Shockey, E. L. Frey, and S. E. H. Sakimoto (2002), Ancient lowlands on Mars, *Geophys. Res. Lett.*, *29*(10), 1384, doi:10.1029/2001GL013832.

Frey, H., L. Edgar, and R. Lillis (2007), Very large visible and buried impact basins on Mars: Implications for internal and crustal evolution and the Late Heavy Bombardment in the inner solar system, in *Seventh International Converence on Mars*, *LPI Contrib. 1353*, 3070, Lunar and Planet. Inst., Houston, Tex.

Gomes, R., H. F. Levison, K. Tsiganis, and A. Morbidelli (2005), Origin of the cataclysmic Late Heavy Bombardment period of the terrestrial planets, *Nature*, *435*, 466–469, doi:10.1038/nature03676.

Hartmann, W. K., and G. Neukum (2001), Cratering chronology and the evolution of Mars, *Space Sci. Rev.*, *96*, 165–194.

Holsapple, K. A. (1993), The scaling of impact processes in planetary sciences, *Annu. Rev. Earth Planet. Sci.*, *21*, 333–373, doi:10.1146/annurev.ea.21.050193.002001.

Hood, L. L., N. C. Richmond, E. Pierazzo, and P. Rochette (2003), Distribution of crustal magnetic fields on Mars: Shock effects of basin-forming impacts, *Geophys. Res. Lett.*, *30*(6), 1281, doi:10.1029/2002GL016657.

Jellinek, A. M., A. Lenardic, and M. Manga (2002), The influence of interior mantle temperature on the structure of plumes: Heads for Venus, Tails for the Earth, *Geophys. Res. Lett.*, *29*(11), 1532, doi:10.1029/2001GL014624.

Johnson, C. L., and R. J. Phillips (2005), Evolution of the Tharsis region of Mars: Insights from magnetic field observations, *Earth Planet. Sci. Lett.*, *230*, 241–254.

Kuang, W., W. Jiang, and T. Wang (2008), Sudden termination of Martian dynamo?: Implications from subcritical dynamo simulations, *Geophys. Res. Lett.*, *35*, L14204, doi:10.1029/2008GL034183.

Lillis, R. J., H. V. Frey, and M. Manga (2008a), Rapid decrease in Martian crustal magnetization in the Noachian era: Implications for the dynamo and climate of early Mars, *Geophys. Res. Lett.*, *35*, L14203, doi:10.1029/2008GL034338.

Lillis, R. J., H. V. Frey, M. Manga, D. L. Mitchell, R. P. Lin, M. H. Acuña, and S. W. Bougher (2008b), An improved crustal magnetic field map of Mars from electron reflectometry: Highland volcano magmatic history and the end of the Martian dynamo, *Icarus*, *194*, 575–596, doi:10.1016/j.icarus.2007.09.032.

Marinova, M. M., O. Aharonson, and E. Asphaug (2008), Mega-impact formation of the Mars hemispheric dichotomy, *Nature*, *453*, 1216–1219, doi:10.1038/nature07070.

McKinnon, W. B., and P. M. Schenk (1985), Dark halo craters and the thickness of grooved terrain on Ganymede, in *Lunar Planet. Sci.*, vol. XVI, pp. 544–545.

McKinnon, W. B., P. M. Schenk, and J. M. Moore (2003), Goldilocks and the three complex crater scaling laws, in *Impact Cratering: Bridging the Gap Between Modeling and Observations*, *LPI Contrib. 1155*, 48 pp., Lunar and Planet. Inst., Houston, Tex.

Melosh, H. J. (1989), *Impact Cratering: A Geologic Process*, *Oxford Monogr. Geol. Geophys.*, vol. 11, 253 pp., Oxford Univ. Press, New York.

Melosh, H. J. (2008), Did an impact blast away half of the Martian crust?, *Nature Geosci.*, *1*, 412–414, doi:10.1038/ngeo237.

Monteux, J., N. Coltice, F. Dubuffet, and Y. Ricard (2007), Thermo-mechanical adjustment after impacts during planetary growth, *Geophys. Res. Lett.*, *34*, L24201, doi:10.1029/2007GL031635.

Mustard, J. F., F. Poulet, J. W. Head, N. Mangold, J.-P. Bibring, S. M. Pelkey, C. I. Fassett, Y. Langevin, and G. Neukum (2007), Mineralogy of the Nili Fossae region with OMEGA/Mars Express data: 1. Ancient impact melt in the Isidis Basin and implications for the transition from the Noachian to Hesperian, *J. Geophys. Res.*, *112*, E08S03, doi:10.1029/2006JE002834.

Neumann, G. A., M. T. Zuber, M. A. Wieczorek, P. J. McGovern, F. G. Lemoine, and D. E. Smith (2004), Crustal structure of Mars from gravity and topography, *J. Geophys. Res.*, *109*, E08002, doi:10.1029/2004JE002262.

Nimmo, F., and D. J. Stevenson (2000), Influence of early plate tectonics on the thermal evolution and magnetic field of Mars, *J. Geophys. Res.*, *105*(E5), 11,969–11,979.

Nimmo, F., and K. Tanaka (2005), Early crustal evolution of Mars, *Annu. Rev. Earth Planet. Sci.*, *33*, 133–161.

Nimmo, F., S. D. Hart, D. G. Korycansky, and C. B. Agnor (2008), Implications of an impact origin for the martian hemispheric dichotomy, *Nature*, *453*, 1220–1223, doi:10.1038/nature07025.

Olson, P. L., and U. R. Christensen (2002), The time-averaged magnetic field in numerical dynamos with non-uniform boundary heat flow, *Geophys. J. Int.*, *151*, 809–823.

O'Reilly, W. (1984), *Rock and Mineral Magnetism*, 220 pp., Chapman and Hall, New York.

Reese, C. C., and V. S. Solomatov (2006), Fluid dynamics of local Martian magma oceans, *Icarus*, *184*, 102–120, doi:10.1016/j.icarus.2006.04.008.

Reese, C. C., V. S. Solomatov, and J. R. Baumgardner (2002), Survival of impact-induced thermal anomalies in the Martian mantle, *J. Geophys. Res.*, *107*(E10), 5082, doi:10.1029/2000JE001474.

Shahnas, H., and J. Arkani-Hamed (2007), Viscous and impact demagnetization of Martian crust, *J. Geophys. Res.*, *112*, E02009, doi:10.1029/2005JE002424.

Stanley, S., L. Elkins-Tanton, M. T. Zuber, and E. M. Parmentier (2008), Mars' paleomagnetic field as the result of a single-hemisphere dynamo, *Science*, *321*, 1822–1825.

Stevenson, D. J. (2003), Planetary magnetic fields, *Earth Planet. Sci. Lett.*, *208*, 1–2, doi:10.1016/S0012-821X(02)01126-3.

Tan, E., E. Choi, P. Thoutireddy, M. Gurnis, and M. Aivazis (2006), GeoFramework: Coupling multiple models of mantle convection within a computational framework, *Geochem. Geophys. Geosyst.*, *7*, Q06001, doi:10.1029/2005GC001155.

Tonks, W. B., and H. J. Melosh (1992), Core formation by giant impacts, *Icarus*, *100*, 326–346, doi:10.1016/0019-1035(92)90104-F.

Wanke, H., and G. Dreibus (1994), Chemistry and accretion history of Mars, *Philos. Trans. R. Soc. London, Ser. A*, *349*, 285–293.

Watters, W. A., M. T. Zuber, and B. H. Hager (2009), Thermal perturbations caused by large impacts and consequences for mantle convection, *J. Geophys. Res.*, *114*, E02001, doi:10.1029/2007JE002964.

Williams, J. P., and F. Nimmo (2004), Thermal evolution of the Martian core: Implications for an early dynamo, *Geology*, *32*, 97–200.

Zhong, S., M. T. Zuber, L. Moresi, and M. Gurnis (2000), Role of temperature-dependent viscosity and surface plates in spherical shell models of mantle convection, *J. Geophys. Res.*, *105*(B5), 11,063–11,082.

R. J. Lillis, Space Sciences Laboratory, University of California, 7 Gauss Way, Berkeley, CA 94720-7450, USA.

M. Manga, Department of Earth and Planetary Science, University of California, 301 McCone Hall, Berkeley, CA 94720-4767, USA.

J. H. Roberts, Johns Hopkins University Applied Physics Laboratory, 11100 Johns Hopkins Road, Laurel, MD 20723-6099, USA. (james.roberts@jhuapl.edu)